Vietnam Journal of Catalysis and Adsorption
Tạp chí xúc tác và hấp phụ Việt Nam

http://chemeng.hust.edu.vn/jca/

Synthesis of some Bismuth Sulfide nano/micro-structures and reduction catalytic of Cr(VI) under visible light irradiation

Do Thi Anh Thu[1,*], Vu Thi Thai Ha[1], Pham Quang Ngan[1], Giang Hong Thai[1], Nguyen Trung Hieu[2,3], Man Minh Tan[2,3], Hồ Trường Giang[1], Trần Đại Lâm[4]

[1]*Institute of Materials Science, Vietnam Academy of Science and Technology, Hanoi, VIETNAM*
[2] *Institute of Theoretical and Applied Research, Duy Tan University, Hanoi, VIETNAM*
[3] *Faculty of Natural Sciences, Duy Tan University, Da Nang, VIETNAM*
[4] *Institute for Tropical Technology, Hanoi, VIETNAM*
**Email: thudta@ims.vast.vn*

ARTICLE INFO

Received: 15/11/2020
Accepted: 30/12/2020

Keywords:
Bismuth Sulfide, Hydrothermal Method, Cr(VI) photoreduction.

ABSTRACT

Bismuth sulfide (Bi_2S_3) nanostructures with various morphologies, including nanowires, nanorods and nanoflowers, have been successfully fabricated via a facile hydrothermal method. The results show that the sulfur source plays a crucial role in determining the product morphology. Photocatalysis experiments show Bi_2S_3 nanowires exhibit the highest photocatalytic reduction of Cr(VI) when exposed to visible light irradiation.

Introduction

As an important A_2B_3 metal chalcogenide semiconductor with a narrow band gap of 1.3-1.7 eV [1-2], bismuth sulfide (Bi_2S_3) nanostructures have attracted the attention of many scientists around the world because they have potential wide-ranging applications, including photocatalytic [3], thermoelectric [4], gas sensor [5], etc... Among them, one-dimensional (1D) nanostructures are very attractive due to their unique optical, electrical, catalytic and magnetic properties, etc. [6-7]. The synthesis of the semiconductor nanostructures with the controlled size, shape, and morphology is very important from both basic and applied research point of view.

With the advantages of high shape ratio, enhanced light scattering and absorption, fast transport of free electrons along their length and efficient use of electron-hole pairs, the one-dimensional nanostructures exhibited a superior photocatalytic efficiency to others. Therefore, the one-dimensional Bi_2S_3 materials are expected to be applied for environmental treatment.

As industry developed, wastewater from industrial factories was considered the main source of water pollution [8-9]. Hexavalent chromium - (VI) is an extremely toxic heavy metal ion that affects the human body and even the ecosystem because of a high ability to cause cancer and high mutation [10]. Therefore, the removal of Cr(VI) from wastewater is an urgent matter in environmental treatment. Some works have been carried out to deal with Cr(VI)-containing effluents, including chemical precipitation, ion exchange, adsorption... [11]. Among all of these methods, photocatalytic reduction of toxic Cr(VI) to less poisonous Cr(III) is one of the most attractive methods due to its cost-effective and efficient [12]. Cr(VI) - adsorption and conversion are an effective and expected direction in wastewater treatment technology. Bi_2S_3 nanostructures have both adsorption

http://doi.org/10.51316/jca.2020.074

capacity and photocatalytic reduction of Cr(VI) under visible light irradiation, so they are promising in wastewater treatment applications. In this work, we present some nano/micro Bi_2S_3 structures synthesized by a simple hydrothermal method. The results showed that the crystal structure and morphology of the Bi_2S_3 nanostructures depend on the original sulfur source. The photo-reduction experiments of Cr(VI) under visible light irradiation also show the high potential of nano/micro Bi_2S_3 structures in polluted wastewater treatment.

Experimental

Synthesis of Bi_2S_3 nano/micro-structures:

All the chemical reagents are analytical reagents including: bismuth nitrate pentahydrate ($Bi(NO_3)_3{\cdot}5H_2O$), thioglycolic acid ($HSCH_2COOH$), thiourea ($(NH_2)_2CS$), thioacetamide (CH_3CSNH_2), and ethanol.

In a typical synthesis procedure for obtaining sample M1: 0,0005 mol bismuth nitrate was dissolved in 50 mL distilled water under magnetic stirring. A white precipitate appeared immediately. After stirring for about 10 minutes, 0,0015 mol thioglycolic acid was added to the above solution. After stirring for 30 minutes, the yellow transparent solution was transferred into a Teflon-lined stainless steel autoclave, sealed and heated at 180°C for 16 h. After the reaction was completed, the autoclave was cooled to room temperature naturally. The black precipitates were centrifuged, washed several times with distilled water and ethanol and then dried at 60°C for 8 h in air.

Similar experiments were performed but with different sulfur sources - thioglycolic acid, thioacetamide, thiourea, and obtained samples were denoted as M1, M2, M3, respectively.

The crystalline structures of the products were analyzed by a powder X-ray diffractometer (XRD, Siemens D5005). The morphologies of the obtained sample were characterized by field-emission scanning electron microscopy (FESEM, Hitachi S4800).

The specific surface area of the products were estimated using the Brunauer–Emmett–Teller (BET) equation based on the nitrogen adsorption isotherm (77 K) by using an Autochem II 2920 (Micromeritics).

The photocatalytic activities of the as-prepared Bi_2S_3 nanostructures were evaluated by photocatalytic reduction of Cr(VI) under visible-light irradiation of a 300 W halogen lamp (Philips) at 20 cm of distance from the surface of the solution to the bulb. In a typical procedure, 50 mg of Bi_2S_3 photocatalysts were dispersed into 50 mL of $K_2Cr_2O_7$ solutions (40 mg/L). The suspensions were stirred for 1 h in the dark to ensure the adsorption-desorption equilibrium before exposed to visible-light irradiation. The solution was then shined under magnetic stirring, ensuring that the catalyst was evenly dispersed in the $K_2Cr_2O_7$ solution. At each given irradiation time interval, 3 mL of the suspension was collected and centrifuged to remove the photocatalyst, then analyzed by recording UV-vis spectra (Shimazu 2600) used diphenylcarbazide as indicator [13]. Based on the decrease of the absorption maximum (I) at 540 nm, the remaining amount of Cr(VI) (X%) was determined from the expression: X% = (C/C_0) x 100% = (I/I_0) x 100%, in which C_0 and C are initial concentration of Cr(VI) and the concentration at reaction time *t*, respectively; I_0 and I are the absorption maximum at 540 nm of the solution at the beginning and after illumination. To evaluate the reusability of the catalyst, after each photocatalytic test cycle, we collected Bi_2S_3 samples, washed many times with diluted HCl solution, distilled water and ethanol, and finally dried at 60°C for 8 h in air. Then the Bi_2S_3 samples were reused in the next experimental cycle.

Results and discussion

Crystalline structure analyse

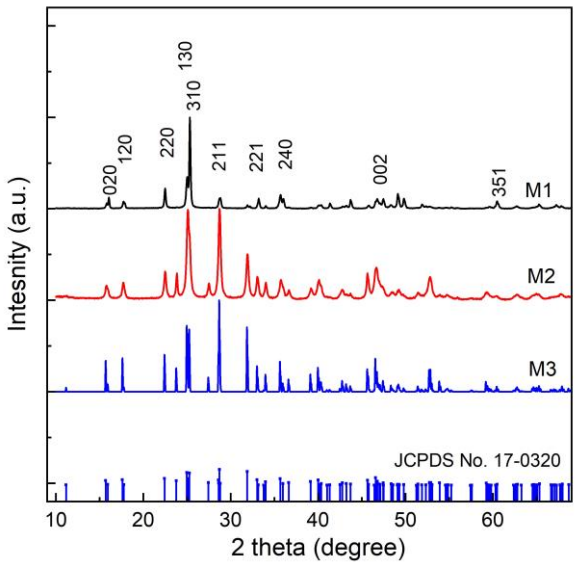

Figure 1: XRD patterns of Bi_2S_3 samples synthesized with different sulfur sources.

The XRD patterns of Bi_2S_3 samples synthesized with different sulfur sources were shown in Fig. 1. All of the diffraction peaks at 15.7°, 17.7°, 22.4°, 24.8°, 25.1°, 28.7°, 31.6°, 46.4°, và 52.6°... can be well indexed to the lattice planes (020), (120), (220), (130), (310), (021), (221),

(002), and (351)... of the standard profile of orthorhombic phase Bi_2S_3 structure (JCPDS No. 17-0320), respectively [14]. No peaks due to impurity or other phases are detected, implying that the final products are of pure phase. However, sample M1 with the highest intensity of diffraction peak at 25.1° compared with the remaining peaks, suggest the preferred orientation in the (310) plane.

Morphology properties of the samples

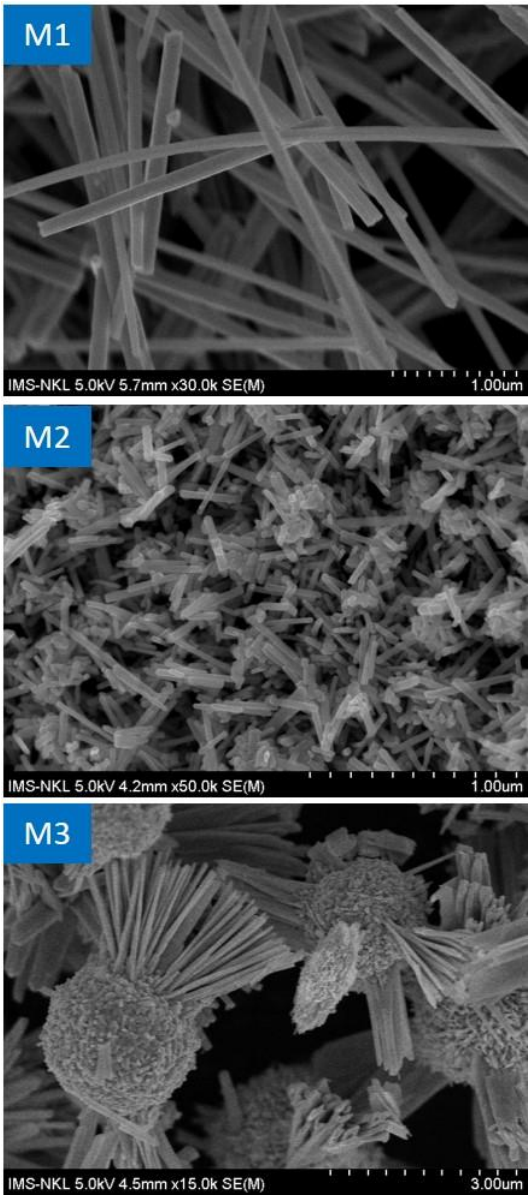

Figure 2: FESEM images for Bi_2S_3 samples synthesized with different sulfur sources.

FESEM images of Bi_2S_3 samples synthesized with different sulfur sources are shown in Fig 2. The results clearly demonstrated that the morphology of the obtained Bi_2S_3 material depends on the sulfur source used initially.

When thioglycolic acid is used, Bi_2S_3 nanowires (M1) are obtained with lengths about several micrometers and widths ranging from 70 to 100 nm. Meanwhile, Bi_2S_3 short nanorods with lenghs of 100-200 nm, widths of 30-50 nm are formed in sample M2 prepared with thioacetamide.

And when the sulfur source is thiourea, the obtained M3 sample possessed a hierarchical structure in which, every hierarchical unit is actually a flowerlike assembly of several nanoparticles and nanoplates, whose size about 3-4 μm. This result shows that the nature of the sulfur source plays an important role in controlling the morphology of Bi_2S_3 nano/micro materials.

Proposed formation mechanisms for the Bi_2S_3 nano/micro structures are as follow:

When using thioglycolic acid, the obtained product is Bi_2S_3 long nanowires. Here, thioglycolic acid as the role of a complexing agent, controls the nucleation and growth of Bi_2S_3 nanowires. The reactions related to the Bi_2S_3 nanowire formation can be expressed as follows:

$$Bi(NO_3)_3 + H_2O \leftrightarrow BiONO_3 + 2HNO_3 \quad (1)$$

$$2BiONO_3 + 3S^{2-} + 2H_2O \leftrightarrow Bi_2S_3 + 4OH^- + 2NO_3^- \quad (2)$$

$$m Bi_2S_3 + k HSCH_2COOH + k Bi^{3+} \leftrightarrow (Bi_2S_3)_m(BiSCH_2COOH)_k^{2+} + kH^+ \quad (3)$$

$$(Bi_2S_3)_m(BiSCH_2COOH)_k^{2+} \leftrightarrow (Bi_2S_3)_m(Bi^{3+})_k + kSCH_2COOH^- \quad (4)$$

$$(Bi_2S_3)_m(Bi^{3+})_k + lS^{2-} \leftrightarrow (Bi_2S_3)_n \text{ (nanowires)} \quad (5)$$

The reaction (1) shows the hydrolysis of bismuth nitrate $Bi(NO_3)_3$, which leads to a white precipitate of $BiONO_3$. Since Bi_2S_3 has a much smaller solubility product than $BiONO_3$, when S^{2-} ions are introduced, Bi_2S_3 precipitates will be formed as the reaction (2). They are the seeds to form Bi_2S_3 nanowire in the next hydrothermal process.

Since Bi_2S_3 has a typical lamellar structure with strong chemical bonds along the *c*-axis and weak van der Waals bonds between layers, this leads to a tendency of preferential growth along the *c*-axis [15]. Therefore, it can be understood that the formation of Bi_2S_3 nanowires in the conventional hydrothermal process includes reactions (1) and (2). According to reported paper [16], reactions (3) - (5) are proposed.

The formation of $(Bi_2S_3)_m$ $(BiSCH_2COOH)_k^{2+}$complex clusters through reaction (3) reduces free Bi2S3 seeds in solution. Reactions (4) and (5) take place during the hydrothermal process. Thus, thioglycolic acid acts as a

"soft template" for the growth of Bi2S3 nanowires (sample M1 - Figure 2).

In an aqueous solution, acetamide hydrolyzes to yield S^{2-} ions (reaction (6)). When it is added into the bismuth nitrate solution, an amorphous precipitate is formed (similar to reactions (1) and (2)). With the increasing of hydrothermal temperature, the amorphous precipitates turns into Bi_2S_3 crystal seeds in the reaction system. In the hydrothermal process, Bi_2S_3 seeds grow along the favorable direction (ie, the direction of the *c*-axis) to form Bi_2S_3 nanorods (reaction (7)) (sample M2 - Figure 2).

The chemical reactions that occur during the synthesis process are (1), (2) and:

$$CH_3CSNH_2 + H_2O \rightarrow CH_3CONH_2 + 2H^+ + S^{2-} \quad (6)$$

$$nBi_2S_3 \rightarrow (Bi_2S_3)_n \text{ (nanorods)} \quad (7)$$

When thiourea $(NH_2)_2CS$ is used, due to thiourea can form a Bi-thiourea complex, prevent uncontrollable formation of Bi_2S_3 (because Bi_2S_3 has a much smaller solubility product than $BiONO_3$, when S^{2-} ions are introduced, Bi_2S_3 precipitation occurred, as described in reaction (7)). The whole forming mechanism is represented by the following reactions:

$$Bi^{3+} + n(NH_2)_2CS \leftrightarrow [Bi((NH_2)_2CS)_n]^{3+} \quad (8)$$

$$(NH_2)_2CS + 2H_2O \leftrightarrow 2NH_3 + CO_2 + 2H^+ + S^{2-} \quad (9)$$

$$nBi_2S_3 \leftrightarrow (Bi_2S_3)_n \text{ (hierarchical structures)} \quad (10)$$

Before the hydrothermal process, the dissociation of S^{2-} ion from thiourea is significantly slow, so the formation of Bi_2S_3 complex seeds is quite limited. After that, the hydrothermal process is started, the dissociation of S^{2-} ions is enhanced at high temperature and high pressure resulting in the formation of many Bi_2S_3 crystal seeds. Because of being formed at a high rate, it is inevitable that the Bi_2S_3 crystal seeds agglomerate somewhere, formed Bi_2S_3 hierarchical structure as shown in Figure 2 (sample M3).

The results of the Cr(VI) photocatalytic reduction experiments under visible light irradiation

The catalytic performances of the samples were estimated through photocatalytic reduction of Cr(VI) to Cr(III) under visible light irradiation. Figure 3 reveals the results of the photocatalytic test under the visible light irradiation of 3 Bi_2S_3 samples.

The blank test (without photocatalyst) showed too small photolysis under 90 min's visible light exposure, indicating that Cr(VI) solution was quite stable under visible light irradiation

All of three Bi_2S_3 samples had adsorption phenomena. After 60 minutes of stirring in the dark, 33% Cr(VI) has been adsorbed onto Bi_2S_3 wires (M1), while the rod sample, this amount was 21.4% and the hierarchical structure, 15.9%. After irradiation for 90 minutes, nearly 95% of Cr(VI) is photocatalytically reduced by Bi_2S_3 nanowires (M1), whereas the other sample as nanorods (M2) and hierarchical structures (M3) exhibit lower activities with a removal rate of about 62 and 48%, respectively. It means the remaining amounts of Cr(VI) in the solution were 5, 38 and 52% corresponding to M1, M2 and M3 samples.

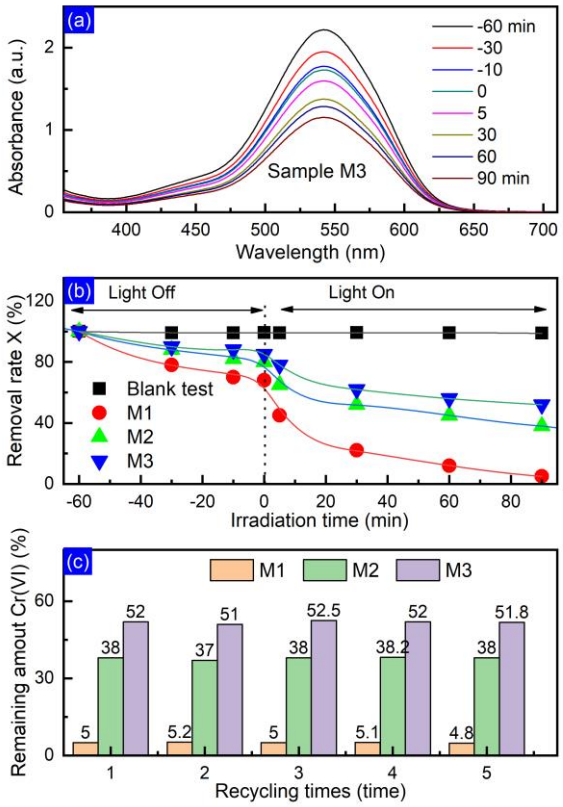

Figure 3: The results of the Cr(VI) photocatalytic reduction experiments under visible light irradiation: (a): UV-visible absorption spectra for photocatalytic reduction of 40 mg/L Cr(VI) using Bi_2S_3 (M3 sample); (b): Photocatalytic reduction of Cr(VI) under visible light irradiation with Bi_2S_3 samples; (c): Remaining amount of Cr(VI) (%) under visible light irradiation within 90 min at reusability experiments of the regenerated Bi_2S_3 photocatalysts.

This result shows that Bi_2S_3 in form of long wire has the highest photocatalytic efficiency among the three samples. The photocatalytic properties are related to the surface area of the catalyst. The BET surface areas

of three Bi_2S_3 samples (M1, M2, M3) are 15.6, 6.9 and 4.3 m^2/g, respectively. Therefore, the enhanced photocatalytic activity may be related to the uniqueness of the ultra-long Bi_2S_3 wire structure, resulting in larger porosity and larger surface area than the rest of the samples. Furthermore, nanowires exhibit a very high respect ratio, enhance light scattering and absorption, rapid transport of free electron along the long axis and efficient electron-hole utilization [17].

The stability of the photocatalyst is one of the key factors to limit the application of photocatalytic technology. The reusability of Bi_2S_3 samples has also been studied by collecting and reusing the same photocatalyst after 5 cycles (Figure 3c).

After the photocatalytic reduction of Cr(VI), formed $Cr(OH)_3$ would be deposited on the surface of the Bi_2S_3 materials, which occupied photocatalytic sites, resulting in a decrease in photocatalytic activity when it has been reused. To overcome this, we washed the sample several times with diluted HCl solution (0.5 M), distilled water, ethanol and then, dried at 60°C for 8 h in air. After refreshing the material's surface, continuing the other test. Figure 3c shows that there is an insignificant change in the photocatalytic activity, the results relatively repeated after each cycle. This shows that Bi_2S_3 material has optical stability and long-term usability.

A mechanism can be proposed based on the optical characteristics of the Bi_2S_3 photocatalyst. With an optical band gap of 1,3-1,7 eV, Bi_2S_3 [1] absorbs easily visible light to generate an electron-hole pair: electrons in the valence band are excited to the conduction band, while created holes in the valence band (equation (11)). Photogenerated electrons and holes migrate to the surface's material to participate in redox reactions. Reaction of photogenerated electrons with surface adsorbed chromate on the photocatalyst surface leads to the formation of Cr(III) (equation (12)) and photogenerated holes oxidize to oxygen as equation (13):

$$Bi_2S_3 + h\nu \rightarrow h_{VB}^+ + e_{CB}^- \quad (11)$$

$$Cr_2O_7^{2-} + 14H^+ + 6e^- \rightarrow 2Cr^{3+} + 7\,H_2O \quad (12)$$

$$2H_2O + 4\,h_{VB}^+ \rightarrow O_2 + 4H^+ \quad (13)$$

Conclusion

By using a simple hydrothermal method, we have fabricated Bi_2S_3 nano/micro structures in form of wires, rods and hierarchical flower. Experimental results also indicate that sulfure source plays important role in determining the morphologies of Bi_2S_3 products.

Bi_2S_3 nano/micro samples were tested in photo-catalytic reduction of Cr(VI) under visible light irradiation. The results showed that the Bi_2S_3 nanowires have the best photocatalytic activity. These nanowires show optical stability and long-term usability.

With these initial results, we will develop further ideas on Bi_2S_3 nanostructures to apply them in the field of photocatalysis for environmental treatment.

Acknowledgments

This work was financially supported by a grant from the National Foundation for Science and Technology Development (NAFOSTED, code: 104.03-2018.312).

References

1. J. Chen, V. Nalla, G. Kannaiyan, V. Mamidala, W. Ji, J. Vittal, New J. Chem. 38 (2014) 985–992. https://doi.org/10.1039/C3NJ01380D
2. Z. Zhu, S. K. Iyemperumal, K. Kushnir, A. D. Carl, L. Zhou, D. R. Brodeur, R. L. Grimm, L. V. Titova, N. A. Deskins and P. M. Rao, Sustainable Energy & Fuels 1 (2017) 2134-2144.
3. T. Wu, X. Zhou, H. Zhang, X. Zhong, Nano Res. 3 (2010) 379-386. https//doi.org/10.1007/s12274-010-1042-0
4. Z. Ge, P. Qin, D. He, X. Chong, D. Feng, Y. Ji, J. Feng, J. He, ACS Appl.Mater. Interfaces 9(5) (2017) 4828–4834. https://doi.org/10.1021/acsami.6b14803
5. H. Li, J. Yang, J. Zhang, M. Zhou, RSC Adv. 2 (2012) 6258–6261. https://doi.org/10.1039/C2RA20751F
6. F. Lu, R. Li, Y. Li, N. Huo, J. Yang, Y. Li, B. Li, S. Yang, Z. Wei, J. Li, ChemPhysChem 16 (2015) 99–103.
7. Q. Yang, C. Hu, S. Wang, Y. Xi, K. Zhang, J. Phys. Chem. C 117(11) (2013) 5515–5520. https://doi.org/10.1039/C5CS00838G
8. H. Kyung, J. Lee, W. Choi, Environ. Sci. Technol. 39 (2005) 2376–2382. https://doi.org/10.1021/es0492788
9. G. Zhang, D. Chen, N. Li, Q. Xu, H. Li, J. He, J. Lu, J. Colloid Interface Sci. 514 (2018) 306–315.
10. J. Zhao, Q. F. Han, J. W. Zhu, X. D. Wu, X. Wang, Nanoscale 6 (2014) 10062–10070. https://doi.org/10.1039/C4NR03152K
11. S. Luo, F. Qin, Y. Ming, H. Zhao, Y. Liu, R. Chen, J. Hazard. Mater. 340 (2017) 253–262. https://doi.org/10.1016/j.jhazmat.2017.06.044
12. L. Wang, X. Li, W. Teng, Q. Zhao, Y. Shi, R. Yue, Y. Chen, J. Hazard. Mater. 244 (2013) 681–688. https://doi.org/10.1039/C3CE41481G
13. X. Yuan, Z. Chao, Q. Jing, T. Qi, Y. Mu, A. Du, Nanomaterials 6(9) (2016) 173. https://doi.org/10.1039/C6CS00218H
14. F.W. Shu, G. Feng, S.Y. Zhong, K.L. Meng, G.J. Zhou, G.Z. Wen, J. Cryst. Growth 282 (2015) 79–84.
15. G. Zhu and P. Liu, Cryst. Res. Technol. 44(7) (2009) 713 – 720. https://doi.org/10.1049/mnl.2020.0177
16. D. Hays, O. I. Mieie, M.T. Nenadovic, V. Swayambunathan, D. Meisel, J. Phys. Chem. 93(11) (1989) 4603-4608. https://doi.org/10.1088/0953-8984/22/2/022201
17. Y. Wang, W. Yang, L. Zhang, Y. Hu, X. W. Lou, Nanoscale 5 (2013) 10864-10867. https://doi.org/10.1039/C3NR03909A